Electronic Journal of Structural Engineering

Original Article

Cite this: DOI:10.56748/ejse.24646

Received Date: 6 June 2024
Accepted Date: 23 December 2024

1443-9255
https://ejsei.com/ejse

Experimental and Numerical Studies on The Behavior of RC Exterior Beam–Column Joints Strengthened with Fiber Sheets Under Cyclic Loads

Qais M. Al-Gabri[a*], Ehab M. lotfy[b], Khaled S. Ragab[c], Manar A. Ahmed[d], Abdel-Rahman M. Naguib[b]

[a] Civil Engineering Department, Faculty of Engineering, Thamar University, Yemen.
[b] Civil Engineering Department, Faculty of Engineering, Suez Canal University, Egypt.
[c] Housing and Building National Research center, Egypt.
[d] Associate professor, Faculty of Engineering- Taibah University, Saudi Arabia,
Associate professor, Faculty of Engineering- Suez Canal University, Egypt
*Corresponding author: gaisaljabri503@gmail.com

Abstract

Beam-column joints are critical regions in reinforced concrete (RC) buildings and are most susceptible to seismic loads. Many retrofitting works using fiber -reinforced polymer (FRP) composites are performed in developed countries. This study combines experimental and numerical methods to assess the seismic behavior of seven RC beam-column joints specimens. Carbon fiber sheet, glass fiber sheet, and hybrid fiber (carbon + glass) were used for strengthening. One control specimen, two carbon wrapping specimens, two glass wrapping specimens, and two hybrid wrapping specimens selected to represent different strengthening schemes. Controlled displacement cyclic loading scenario at a frequency of 0.05 Hz was chosen to simulate seismic loading. Behavior of strengthening joints was studied using the following indices: first cracking and ultimate loads, energy dissipation, ductility, and stiffness. Numerical modeling for the RC beam-column joints specimens using ANSYS software package were created and analyzed. Testing results of different strengthening schemes were compared to both control specimen's results and those from numerical models. Results showed that the hybrid combination was more effective for improving the ductility by 29%, and dissipating energy by 54% of the beam-column joints at a high cost. Furthermore, it was concluded that the proposed numerical model is adequate to describe the behavior of RC exterior beam–column joints strengthened with fiber sheets.

Keywords

Beam–column joint, Hybrid fiber reinforced polymer (HFRP), Cyclic loading, Strengthening, Ductility, Numerical model

1. Introduction

RC structures are constructed for many purposes and functions. A structure is designed to perform its functions. As the number of function intension, the demand for structural expansions increases, to solve this increase. FRP sheets have been commonly utilized for strengthening RC members because of the advantages of these materials, including easy installation, capacity to resist corrosion, high tensile force, and it is lightweight. FRP sheet systems in many projects have been used to a considerable extent during the last few years (Esmaeeli, 2015). In civil engineering, four types of fibers are used: glass, carbon, aramid, and Basalt fibers (GFRP, CFRP, BFRP, and AFRP). In addition, a new technique that uses HFRP sheets to strengthen the RC is recently developed. In fact, several previous studies have shown that concrete damage is concentrated in the connections, mostly in the area close to the beam - column interfaces, and which is liable to gravity loads or earthquakes (Wang et al., 2019). To improve the ductility of the RC structures, switch plastic hinges were thus proposed for beams that were farthest from the faces of the column. This can be achieved by modifying the joint using FRP sheets (Javanmardi & Maheri, 2017). An adequate reinforcement region for the shear percentage region in the beam-column joint zone can prevent shear joint failure during earthquakes (Ghayeb et al.,2020). The shear and flexural behaviors of the joints must also be considered. In RC joints, the shear strength tends to decrease while inelastic flexural displacement high (Shayanfar et al., 2018). Furthermore, the study of joint behavior during inverse cyclic loading earthquakes is required to offer details regarding seismic design (Zeng et al., 2015), such as the strength and stiffness degradation, displacement with load, energy dissipation amplitude, ductility, and confinement in connections (Liu & Jia, 2018). The shapes of the failures are distributed as joint or beam failures. The load capacity was demonstrated through the accidental load (Pmax) utilized in the joint subaggregation and the shear strength of the horizontal mid-height cross-section in the connections (Kotsovou et al., 2017). On the basis of the main reinforcement ratio of the beam, awesome failure modes are anticipated, particularly, failure shear in the joint without beam yielding and the after-beam yielding (Verderame et al., 2018). The increase in the axial load level from 5% to 30% for the column results in an increase in the vertical load capacity for the beam tip because it provides more confinement of the joint core (Aboelhassan, 2020). The major causes of connection failure are the horizontal stirrup ratio, which expresses diagonal cracks, starts yielding, failure from reinforcement installation, damage to the moment loading of columns close to connections, and widening and narrowing of cracks due to cyclic loads (Rahim, 2019). FRP materials are used to strengthen different RC elements to reinforce the shear, flexural, and axial load-carrying capacities of the joints. (Mariselvam & Sakthieswaran, 2015) inspected the seismic behavior of joints using GFRP sheets and found that increasing the number of GFRP layers (1, 2, 3 layers) increased the axial compressive force of the beam-column join by 1.06%, 1.346%, 1.448% respectively. (Nawale et al., 2015) investigated the results of a strengthening technique using a casing system for damaged RC interior connections and proved that it is as effective as the stiffness and ultimate load of the strengthened beam decreases with displacement. (Mosallam et al., 2019) comprehensively studied eight full-scale interior RC connection specimens for external strengthening and repair. Three methods were selected: high-strength composite sheets (carbon/epoxy), high-modulus sheets, and external sheets. These results prove that FRP composites are the best substitution technique for rehabilitation.

(Khashi et al., 2018) used a numerical model to optimize the dimensions of FRP sheets bonded externally to a concrete joint to obtain an optimal size for the fiber sheet dimensions. The particle swarm optimization algorithm was applied in this study. The results confirmed that the maximum essential optimization factors are the width and thickness of the FRP sheets. (Akhlaghi et al., 2020) investigated different installation methods applied to CFRP -flexural -retrofitted external RC joints. The authors summarized the results of evaluating the extraordinary anchorage methods supplied for the longitudinal fiber sheet installed on of the beam and nearer to the column face. The strength and energy dissipation values increased by 23% and 31%, respectively. In addition, the parametric results indicated that the strength increased upon 54% and 85% by increasing the length (450 to 600 mm) of the FRP sheets. (Gnanapragasam et al., 2016) experimental investigated the connections between reference and retrofitted specimens. The results showed that the first cracking load was 125% for RCC connection specimens repaired with

HFRP (BFRP + GFRP) sheets and 100% for specimens repaired using BFRP sheets. Compared with the reference specimen, the ultimate load increased by 60% for connection specimens repaired with HFRP (BFRP + GFRP) sheets and 20% for specimens repaired using basalt fiber sheets. In addition, compared with the control specimen, the hybrid fiber sheets (BFRP +GFRP) were more effective at treating joints. (Elsouri & Harajli, 2015) studied plastic hinging and flexural failure of beams due to large drift reflexions, which were rehabilitated and strengthened with fiber sheets to restore their function. The proposed technique was successful in repairing damaged connection support and restoring stiffness under lateral forces. (Borujerdi et al., 2021) studied the seismic effect of exterior joints and found a decrease of 33% in the number of connection strips compared with the specific number of connection strips in ACI 318. In addition, we increased the energy dispersion to 30% and the damped ratio to 45% [19].

(Okahashi & Pantelides, 2017) studied strut-and-tie models (STM) for RC connections with less than required reinforcement and homogeneous connections retrofitted using CFRP composite plates. The retrofitted connection realized a 5.0% drift ratio prior to a flexible failure happened; the retrofitted connection had 90%, drift ratio, and the original connection had 95% of the experimental shear. Evaluating the RC connection of seismic effects, such as crack behavior, stiffness and strength retraction, displacement hysteresis, and drift ratio, is necessary to thoroughly examine them, in addition to the shear deformation in the connection and the strain development in the reinforcement (Sasmal & Voggu, 2019). (Faleschinia et al., 2017) performed an experimental study on damaged RC joints and strengthened FRP sheets. in their study, two exterior joints, which were early collapsed under reverse loading and strengthened specimens, demonstrated less initial stiffness than the original joints and dissipated energy by the strengthened specimen had 70% and 58% from the original specimens, respectively. (De Risi et al., 2020) tested weak joints strengthened using different FRP methods, the 4%- 6% drift cycles were described by marked degradation of the specimens due to the shear failure. (Zerkane et al., 2019) studied the cyclic loading effect of CFRP enveloped RC joints, 6 specimens were tested, two of which were reference specimens, and 4 specimens were retrofitted by CFRP. The proposed method has been proven to improve the behavior and final failure shape of the joint. (Marimuthu & Sivasankara Pillai, 2021) studied the joint exterior strengthened by FRP. The FRP reached the ultimate strain without collapse under compression and tension. The strengthen joints demonstrated 67.5 % higher loading, and the results verified that the recommended strengthened systems were successful in restoring the strength capacity as well as the seismic performance, including ductility and strength. (Arowojolu et al., 2019) studied the plastic hinge conversion of an RC joint using CFRP under cyclic loading. The results displayed that CFRP sheets 200 mm length achieved satisfactory results. (Laseima et al., 2021) experimentally studied three homogeneous joints without strips and tested them under cyclic loads that emulated seismic loads. Results showed that the moment capacity and displacement of the BFRP- and CFRP-strengthened samples increased by 61.7%, 55.5%, 58.2% and 31.6%, respectively, compared with the reference sample. (Ilia et al., 2020) experimentally tested strong beam–weak column joint specimens strengthened by CFRP sheets. The results showed good ductility and minimal damage, indicating the effective execution of the modern method used to improve the seismic behavior of these poorly detailed joints under large displacement. (Shen et al., 2021) experimentally tested the seismic behavior of RC connections strengthened by BFRP sheets. In particular, six RC interior connections, including one control specimen and five specimens, were strengthened with BFRP sheets using different methods under cyclic loading. The findings showed that strengthening joints with three layers or a length of two layers is the most efficient way to increase the energy capacity. The rehabilitation of RC joints with FRP sheets improved the shear and increased the energy dispersion (GAYAKE & DHAKE, 2021).

In this study, seven RC exterior joints were tested; one reference specimen, 4 specimens for strengthening by CFRP and GFRP sheets, and two specimens for strengthening by HFRP under cyclic load. The seismic execution of the exterior joints through cracking loads (initial, ultimate), energy dissipation, ductility, and ultimate stiffness was also tested.

2. Experimental program

2.1 Specimens and materials

Seven scale (1:3) RC exterior specimens were tested in this experimental study, and joints designed as specimens BCJ1 to BCJ7 were tested in accordance with the ECP 203-2007 (Egyptian code) (ECP203. 2007) and requirements the recommendation of ACI 318-14 (ACI. 2014) respectively. The structure had a plan of 20×25 m, distance between columns 5 m, a floor height of 3 m, and a total height of 36 m. The Egyptian code for loads and forces ECP 201-2012 was used to determine the seismic design forces. The details of the structure and exterior joint are shown in Fig. 1. The seismic design forces were obtained according to the Egyptian code for loads and forces ECP 201-2012 (ECP 201, 2012). It was assumed that the frames were sufficiently ductile to resist seismic loads. The scale was 1:3 of the structure in the original geometric shape for through the ACI T1.1R-01 (ACI T1.1R-01, 2001) and the size impact was compared by (Barbhuiya & Choudhury, 2015). All specimens had identical dimensions: column cross-section was 100x230 mm, its total length was 1000 mm, beam cross-section was 200x100 mm and its length was 800 mm, as shown in Figs. 2 and 3. The main reinforcement of the column 6 ϕ10mm, and yield strength of 540 N/mm2. Using the main reinforcement of the beam 4 ϕ10mm with a yield strength of 530 N/mm2. Stirrups were used for the column and the beam ϕ6 mm with yield strength of 400 N/mm2. The details of the control specimen are shown in Fig. 2, and the FRP strengthening details of the specimens are given in Table 1.

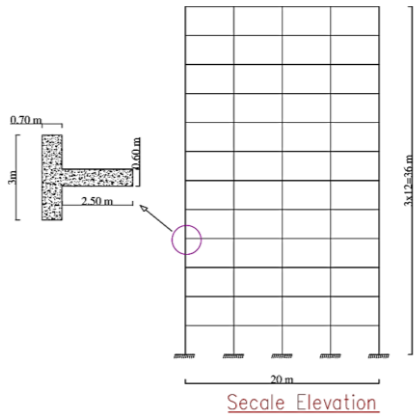

Fig. 1 Layout of a twelve-stored building

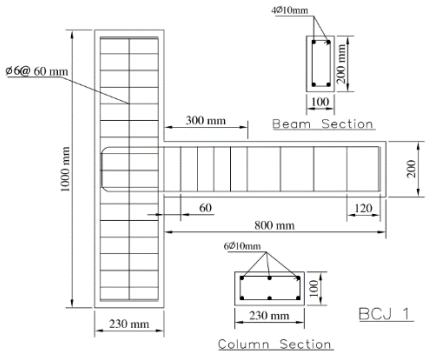

Fig. 2 Reinforcement detailing of the joint

Fig. 3 Beam -column joints molds

Ordinary Portland cement type I (Sinai Cement grade 42.5 N) conforming to the Egyptian Standard Specifications (Specifications, 2009), normal siliceous sand, mashed pink tough limestone aggregate a 10 mm size, and clean water were used in all specimens. The British method was followed when developing the mix design to obtain a concrete resistance of 30 N/mm2. A compression test was conducted on the cub specimens after 28 days, with a mix ratio of 1: 1.81: 3.51 using weight, and a water to cement ratio equal to 0.46. Tables 2 provides the concrete mix proportions necessary to achieve a strength of 30 N/mm2. The concrete was placed into the molds immediately after mixing and leveling of the surface as shown in Fig. 4. Six specimens were strengthened using CFRP, GFRP, and HFRP. CFRP was also applied as a single layer, including GFRP and HFRP with epoxy resin. The constitutive properties of the FRP sheets and epoxy resins are listed in Tables 3 and 4, and details of FRP composites used as shown in Fig. 5.

Table 1. FRP strengthening details of the specimens

Specimens Strengthen	Type of FRP	No. of layer	Strips width (mm)	Loads
BCJ 1-Control	-	-	-	
BCJ2	CFRP	1	50 and 100	
BCJ3	CFRP	1	200 and 250	Gravity
BCJ4	GFRP	1	50 and 100	Loads &
BCJ5	GFRP	1	200 and 250	Cyclic
BCJ6	HFRP	1	50 and 100	Loads
BCJ7	HFRP	1	200 and 250	

Note: The specimens (BCJ2 to BCJ7) have the same dimensions and reinforcement the BCJ1

Table 2. Mix proportions and compressive strength of the specimens

Mix. m3	Fine aggregate (kg/m3)	Coarse aggregate (kg/m3)	Cement content (kg/m3)	w/c ratio	Water (Lit)	Grade of Concrete N/mm2
1	636	1272	350	0.46	160	30

Fig. 4 Concrete specimens casting and moistening

Table 3. Properties of used fibers

Material	Fiber Density (g/cm3)	strength of Fiber Tensile (MPa)	E-Modulus of Fiber Tensile (MPa)	Fiber design thickness (mm)	Strain at break of fibers (%)
Sika CFRP (Wrap_300C)	1.8	3900	230,000	0.17	1.5
Sika GFRP (Wrap-_430G)	2.51	2300	74000	0.17	2.5

Table 4. Properties of the bonding material (Epoxy resin) used

Material	Tensile strength (MPa)	Tensile E-Modulus (MPa)	Applied thickness (mm)	Strain at break of fibers (%)
Sikadur_330	30	4500	0.6	1.2

(a) (b) (c)

Fig. 5 Details of FRP composites used: (a) GFRP (Sika Wrap-_430G) b) CFRP (Sika Wrap_300C) (c) Sikadur-330 adhesive material (epoxy A&B)

2.2 Rehabilitation scheme

The strengthening technique consisted of one layer applying (Small strips 50 mm and 100 mm width, large strips 200 mm and 250 mm width) shaped FRP sheets around the joint. Unstrengthen specimen BCJ1 was left as and control specimen, the specimens BCJ2 to BCJ7 were reinforced by two different methods using FRP sheets. The figure shows 6, the dimensions, and rehabilitation technique general details. Before wrapping the fiber sheets, steps were necessary for all reinforced specimens see Fig. 7. First, the edges of the specimen surfaces were grinded and sanded at the strengthening regions, and the clean and dusty on the surface was removed. Then, mix parts A&B (Resing + Hardener) Sikadur-330 were mixed together in a ratio of 3:1 for at lower 3 min with a mix arm connected to an electrical switch, the material turned into soft and an orderly gray color. Second, the epoxy layer was painted on the sanded areas using a brush, and applied the fiber sheet layer was applied on the joint surface. Finally, the strengthened joints were treated at least 7 days before testing at ambient temperature.

2.3 Test process and loading history

Seven joints (1/3 scaled) were tested in a vertical position, and the devices are illustrated in Figs.8 and 9. All specimens were tested at the concrete and structures research laboratory, Department of Civil Engineering, port said university, Egypt. The column was installed by a group of iron plates and secured to two solid beams through four 18 mm diameter high -strength threaded tie bars, and cyclic loads were applied on the beam tip. Two hydraulic jacks were used to simulate the applied loads (cyclic and axial load). First, a 100 -KN compression jack was used, and an axial load (0.1 $f'c$ Ag) (Zerkane et al., 2019) of the column capacity (55 KN). A 2000-KN hydraulic jack mounted vertically to the loading frame was used to simulate cyclic loads before the beam ends. The electrical pump attached to the jack included an automated valve that controlled the direction and amount of the applied cycle. Experimental tests were performed on all specimens through vertical loads and displacement control at the beam ended according to requirements (ACI T1.1R-01, 2001). The cyclic load was controlled by measuring the beam tip deflection. ±0.5, ±1, ±1.5, ±2, ±2.5, ±3, ±3.5, ±4 to ±40 mm with drift ratios of 0.06%, 0.13%, 0.19%, 0.25%, 0.31%, 0.38%, 0.44%, 0.5% to 5%. Three cycles were used at any loading step with displacement increment, as depicted in Fig. 10.

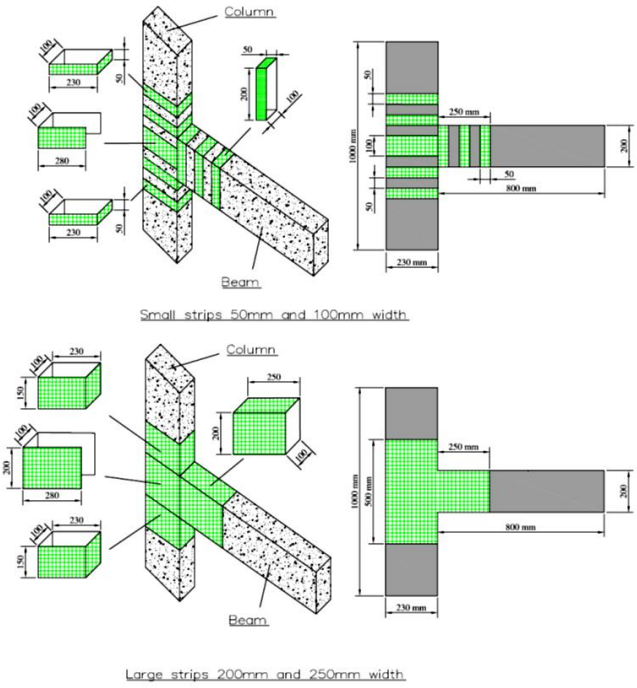

Fig. 6 Strengthening shape of the specimens (BCJ 2 to BCJ 7)

Fig. 7 Preparation and processing strengthening specimens: a) Surface leveling, b) applying primer epoxy layer on surface and installing the FRP sheets, c) Resin putting on FRP sheet, d) placing the strengthened beam column joints for curing

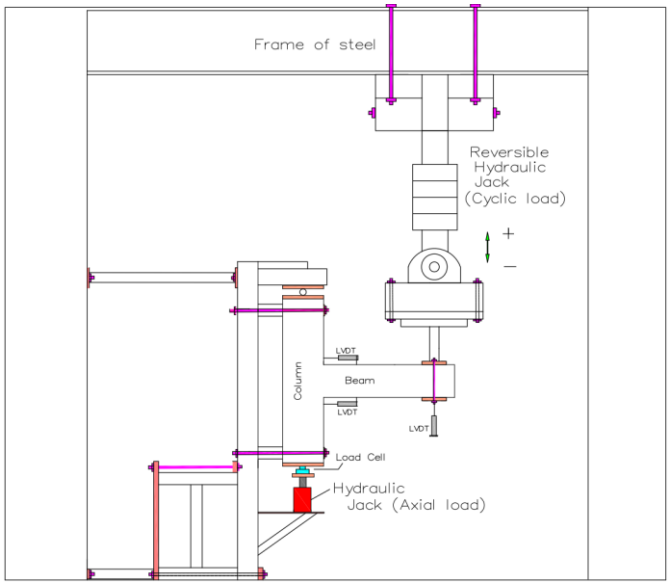

Fig. 8 Test system, boundary conditions for all joints, and sites of LVDTs

Fig. 9 Photo of the loading arrangements and instrumentation

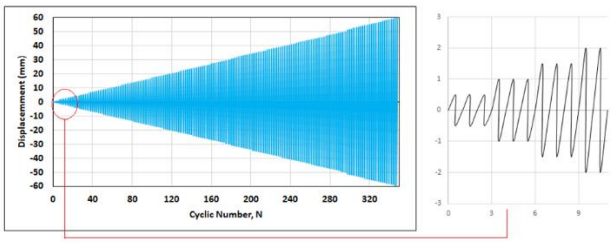

Fig. 10 Vertical cyclic loading history

2.4 Measuring devices

One linear variable differential transducer (LVDT) was connected to the bottom surface of the beam tip, parallel to the load direction, to obtain on displacement, 2 LVDTs were connected on the beam face adjacent to the column to read the concrete strains at the plastic hinge area averaged over a 200 mm range length, and 2 LVDTs were placed vertical on the joint region to estimate the deformation, as depicted in Figs. 8 and 9.

3. Numerical Analysis

Exterior beam- column joint is being modeled and analyzed under cyclic load using ANSYS. It is a numerical technique for finding approximations for a range of engineering problems as well as for solving differential or integral equations. SOLID65 is used to model solids in three dimensions, either with or without reinforcing bars. It was specifically designed for concrete to handle creep, plasticity, cracking under tension, and squeezing under compression. The proposed method assumes the nonlinear function of the solution and obtains the function parameters in a way that reduces the solution's error (Abdulkadir et al., 2017). In this study, a three-dimensional model was created using the ANSYS2019R software. Each element has eight nodes, at each node there are 3 degrees freedom, possess clarifications of a nodal (x, y, z) direction, and behavior the non- linear properties of the elements, required iteration to solve (Mohanan et al.,2016), 8- node solid element using to model the FRP sheet (SOLID 46), and Element LINK 180 is used in the model of reinforcement (Thompson & Thompson, 2017).

3.1 Modeling of exterior joint

Using the program ANSYS engineering tools, we drew models for testing specimens (3D model), solid 65, Link 180, and SOLID 46 using defining materials, mesh size (25 mm), as shown in Fig. 11.

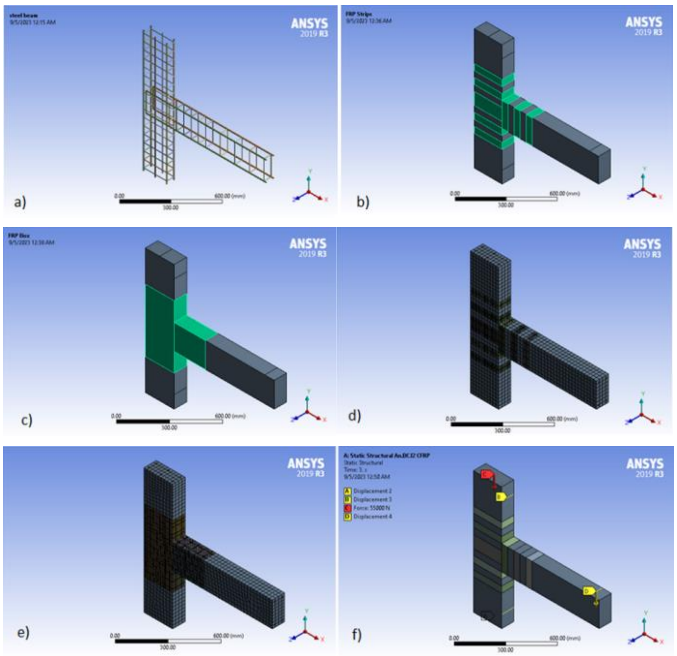

Fig. 11 Modeled specimens: (a) Reinforcement (Link 180), (b) Concrete model (solid 65) strengthened with strips fiber sheets, (c) Concrete model (solid 65) strengthened with box fiber sheets, (d-e) Meshing model, (f) Boundary conditions and loading of the specimens.

3.2 Load and boundary conditions

Axial load on the column (0.1 $f'c$ Ag = 55KN) and cyclic load on the beam. Boundary conditions were utilized in a finite element model that simulates real conditions in the experimental tests and using steel bars at the concrete encirclement, in ANSYS2019R3 utilizes bonded contact, as shown in Fig. 11 (f) and Fig. 12.

3.3 Material properties

The material linear properties and elements used in the modeling described in ECP (203) and ACI 440.R1.06 (ACI. 2014; ECP201. 2012) are listed in Table 5.

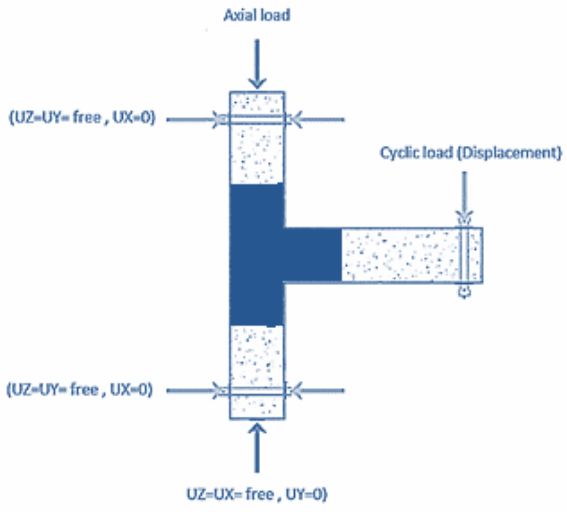

Fig. 12 Application of loads and boundary condition

Table 5. Material properties

Material	Density Kg/m3	Elastic modulus (E_c) MPa	Poisson's ratio (v)	Unconfined compressive strength (f_c) MPa	Tensile strength (f_t) MPa	Yield strength (f_t) MPa	Element used
Concrete	2300	29125	0.2	30	2.90	-	solid 65
Reinforcement steel	7850	$2*10^5$	0.3	-	-	420	Link 180
CFRP	1800	$2.3*10^5$	0.3	-	3900	-	solid 46
GFRP	1850	76000	0.1	-	2300	-	solid 46

4. Results and discussion

4.1 Experimental results

Crack patterns and failure modes

Specimen BCJ1 (control)

In the control specimen, flexural cracking of the beam section under at first appeared under a load of 6.25 KN at 0.26% drift ratio (Δ= 2mm). Cracks were detected by each other beside the beam almost to column. Horizontal cracks in the joint core under a load of 17 KN at 1.68% drift ratio (Δ= 12.6mm). Because of the open and closed sloping and vertical cracks, the fragmenting of the concrete cover started at the bottom of the beam nearer to the column face at a 2% drift ratio (Δ= 15mm), as shown in Fig. 13 (a). Lastly, wide cracks appeared in the joint zone at a load of 18.87 KN at a 5.31% drift ratio (Δ= 39.88mm) due to excessive deformations in the beam connected to the column and plastic hinges in this zone.

Specimens SBC2-SBC7 (strengthened by FRP)

In specimen BCJ2, a final failure is demonstrated in Fig. 13 (b). Flexural cracks nearer to the core region could be observed in the beams at 50 mm away with a load of 16.5 KN, 1.1% drift ratio (Δ = 8 mm), increasing the crack size, while gradually reducing the load. Cracks were discovered in the beam nearer to the column at the load 9.5 KN, and 0.47% drift ratio (Δ = 3.5 mm). Shear cracks appeared in the beam portion at a distance of 300 mm from the joint with a load of 19 KN, and 4.3% drift ratio (Δ = 32 mm). Slanting cracks in the joint region occurred at a load 12.20 KN; and 0.73% drift ratio (Δ = 5.5mm), these cracks were prevented from the beam tips using CFRP strips with a width of 50 mm. In specimen BCJ3, there was a final failure, as shown in Fig. 13 (c). Because CFRP sheets (large strips 200 mm and 250 mm width) using, the initial cracking occurred at a load of 13 KN, displacement of 5 mm, and drift ratio of 0.67%. The shear cracks nearer to the joint area could be observed in the beam with a distance of 400 mm at a load of 15.25 KN and an 0.82% drift ratio (Δ = 6.2 mm). Flexural cracks were observed in beam parts in the joint area. Identically, cracks were noticed in the two aspects due to the applied cyclic load. At the beam tip form nearer to the joint, de-bonding occurred for of CFRP at a load of 19.32 KN, displacement of 12 mm, and 0.73% drift ratio. The degradation in strength progressed and the load was ended as the capacity dropped of the beam with an ultimate load of 21.5 KN at a 5.3% drift ratio (Δmax = 40 mm). We also noticed that a small damage occurred to the joint because of joint strengthening by CFRP sheets on large strips. In specimen BCJ4, there was a final failure, as shown in Fig. 13 (d). Because of GFRP sheets (small strips 50 mm and 100 mm width) using, flexural cracks spotted to joint region, could be seen at beam distance 60 mm at a load of 8.3 KN, 0.4% drift ratio (Δ = 3 mm), with the expansion of the cracks, and while gradually reducing the load. Cracks were discovered in the beam near to the column at a load of 9.65 KN, and 0.47% drift ratio (Δ = 3.5 mm). Shear cracks appeared in the beam portion at a distance of 250 mm from the joint with a load of 12.3 KN at a 0.7% drift ratio (Δ = 5 mm). Slanting cracks in the joint region occurred at load 10.75 KN, and 0.53% drift ratio (Δ = 4 mm) these cracks were prevented from the beam tips using GFRP strips with a width of 50 mm. In specimen BCJ5, there was a final failure, as shown in Fig. 13 (e).

Because of the GFRP sheets (large strips 200 mm and 250mm width) using, the initial cracking occurred at a load of 10.25 KN, displacement of 3.5 mm, and drift ratio of 0.67%. The shear cracks nearer to the joint area could be observed in the beam with a distance of 350 mm at a load of 15.25 KN and an 0.82% drift ratio (Δ = 6.5 mm). Flexural cracks were observed in beam parts in the joint area. Identical cracks were noticed on the two sides because of the cyclic nature of the applied load. At the beam tip form nearer to the joint, de-bonding occurred for the GFRP at a load of 19.32 KN, displacement of 12 mm, and drift ratio of 0.73%. The degradation in strength progressed and the load was ended as the capacity dropped of the beam with an ultimate load of 24.38 KN at a 6.5% drift ratio (Δmax = 49 mm). We also noticed that a small damage occurred to the joints because of the joint strengthening by the GFRP sheet on the large strips shape. Identically, cracks were noticed in the two aspects due to the applied cyclic load. In specimen BCJ6, there was a final failure, as shown in Fig. 13 (f). Because of the HFRP sheets (small strips 50 mm and 100 mm width) using, the first cracking occurred at a load of 11.8 KN, displacement of 4 mm, and drift ratio of 0.53%. Shear cracks nearer to the joint area could be observed in the beam with a distance of 300 mm at load 22 KN at 1.47% drift ratio (Δ = 11 mm). Flexural cracks were observed in beam parts in the joint area. At the beam tip form nearer to the joint, de-bonding occurred for the HFRP at the bottom of the beam nearer to the column face, and the degradation in strength progressed and the load was ended as the capacity dropped of the beam with a maximum load of 23.35 KN at a 5.8% drift ratio (Δmax = 44 mm). In specimen BCJ7, there was a final failure, due to the use of HFRP sheets (large strips 200 mm and 250 mm width) using, the flexural cracks were firstly spotted at the exterior zone of the beams at load 17.5 KN at a 0.9% drift ratio (Δ = 7 mm). Identically, cracks were noticed in the two aspects due to the cyclic load applied nearer to the column. Shear cracks appeared in the beam portion at a distance of 350mm from the joint with a load of 22.3 KN at a 1.3% drift ratio (Δ = 10mm). The slanting cracks in the joint region occurred at load 21.12 KN, and 1.3% drift ratio (Δ = 14 mm). At the beam tip form nearer to the joint, de-bonding of the HFRP occurred in the terminal part of the column face at a load of 18.3 KN and a 4.8% drift ratio (Δ = 36 mm), and the degradation in strength progressed, and the load was ended as the capacity dropped of the beam at a load of 26.87 KN and an 8% drift ratio (Δmax = 59.8 mm), as shown in Fig. 13 (g).

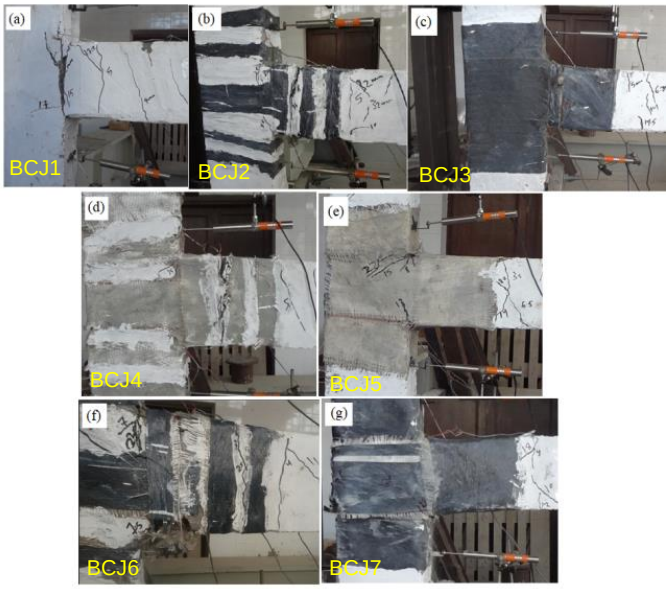

Fig. 13 Final damage and cracking of all test specimens: specimens BCJ1-BCJ7

Hysteretic response and load–displacement curves

Analysis and comparison of load with displacement hysteretic loops. Fig. 14 shows the load- displacement curves of BCJ1 (control), and BCJ2 - BCJ7 (strengthened by FRP). Enveloped area of hysteretic behavior, which is used to evaluate the sample's energy dissipation under cyclic load (Cohn & Riva, 1991). The hysteretic behavior of BCJ1 specimen displayed, early pinching event, which came back to concrete spalling and deterioration in stiffness, as shown in Fig. 14. The hysteretic behavior of BCJ1-BCJ7 displayed full curves and circular, explains that the seismic load of joints was increased due to strengthening by the FRP sheets. Also, BCJ2-BCJ7 showed longer yielding and lower deterioration in the stiffness, compared to BCJ1(control specimen). The hysteretic loop of the joint in term of curve for BCJ1 indicates that BCJ1 reached the maximum beam tip load during the last cycle with a 39.88 mm vertical displacement (5.34% drift ratio). The maximum experimental beam tip loads of this specimen were between +18.87 KN and -18.88 KN. On the other hand, neither axial load degradation nor a significant pinching effect was observed, shown in Fig.14 (a). The maximum loads of specimens BCJ1, and BCJ2-BCJ7 increased by 9.3%, 13.87%, 4.13%, 29.13%, 23.7%, and 42.32% compared with the BCJ1 control specimen, respectively. The envelope curve of the

BCJ1 control was surrounded by the retrofitted specimen's curve, indicating that the bearing capacity and displacements of BCJ2- SBJ7 specimens were higher than those of BCJ1 specimen. The envelope curves the BCJ2-BCJ7 specimens were not similar in of the operations of going up and down as expected, which the test setup's asymmetry may have contributed to. Besides, specimens BCJ6, BCJ7 displayed the largest displacement between these strengthened specimens, indicating that strengthening the joints by HFRP was an effective technique, as depicted in Fig. 15.

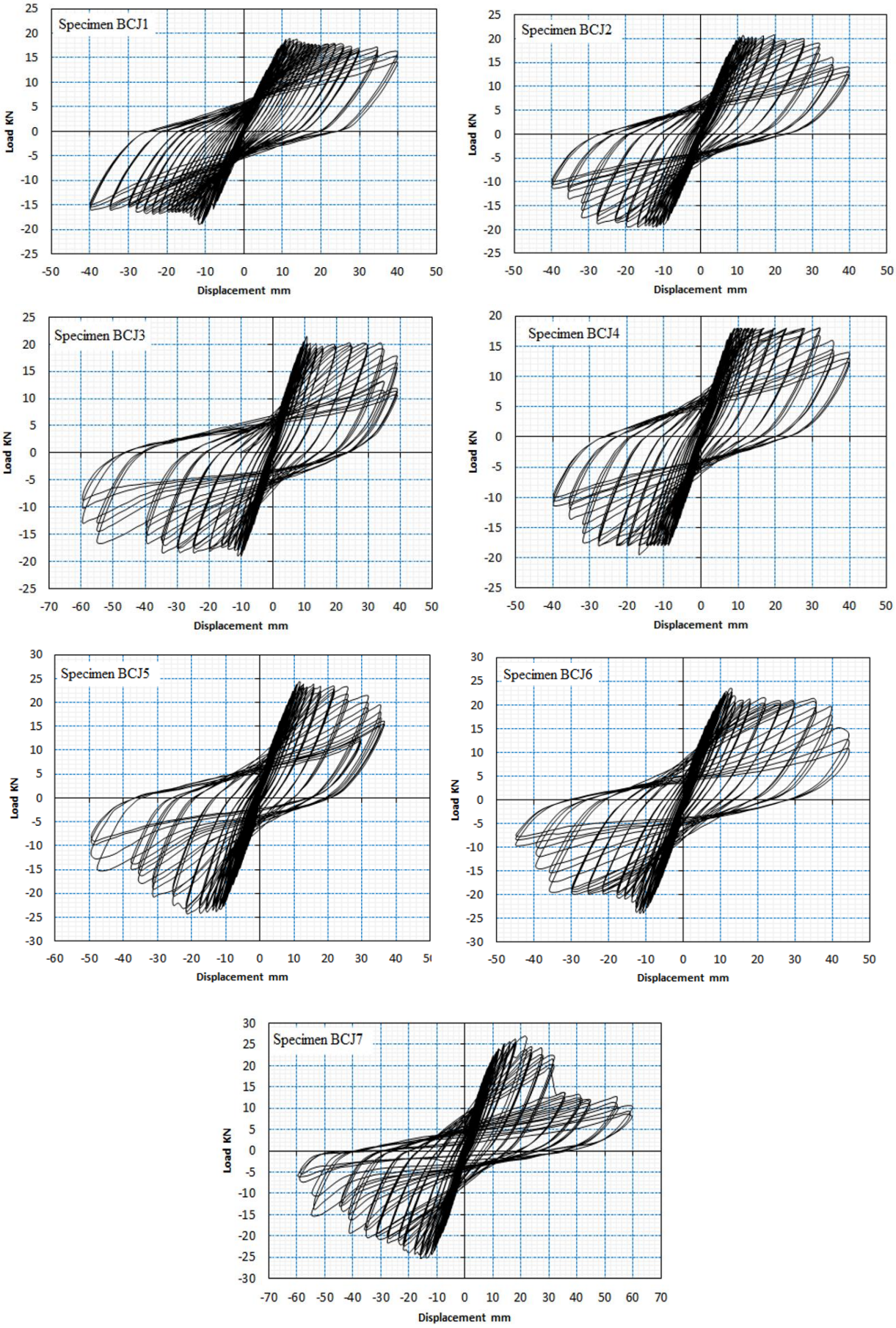

Fig. 14 Load-displacement hysteretic curve of all test specimens BCJ1-BCJ7

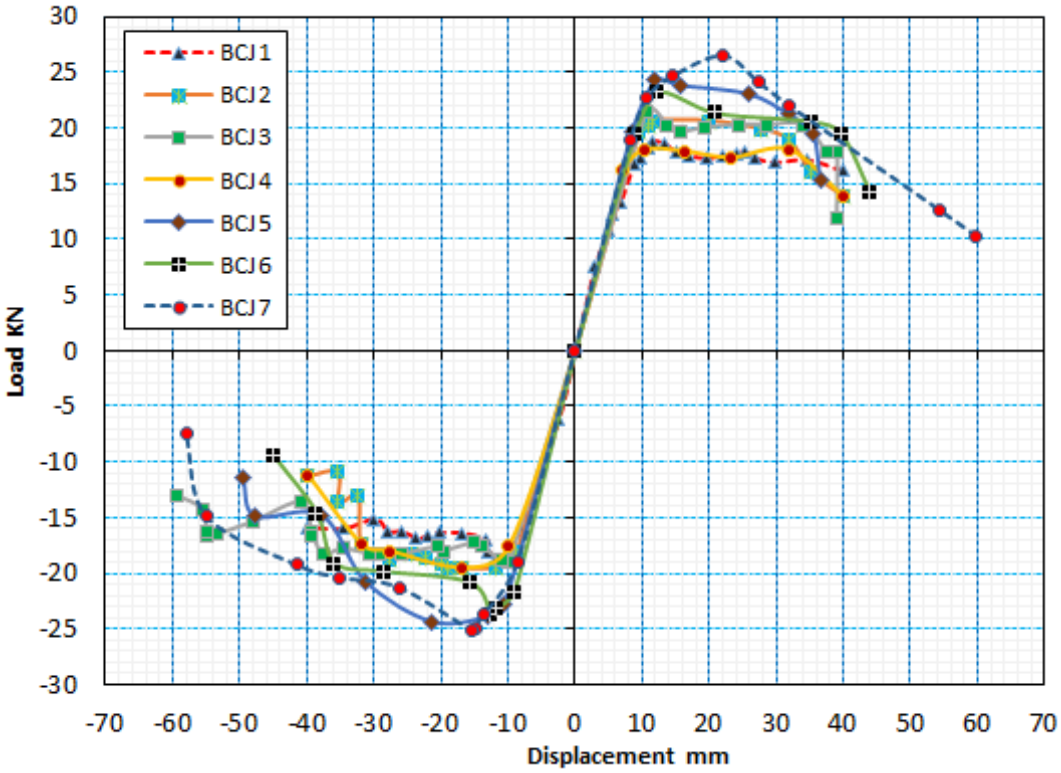

Fig. 15 Envelope of the hysteresis loops of test specimens

Displacement ductility

Table 6. Displacement ductility factor of the BCJ1 - BCJ7 specimens

Specimens	Δ_y (mm)		Δ_u (mm)		(μ)		$\mu_{av.}$	Ultimate Drift ratio (%)
	Positive	Negative	Positive	Negative	Positive	Negative		
BCJ1	7.50	8.10	39.60	39.95	5.28	4.93	5.11	5.28
BCJ2	7.23	7.50	39.90	40	5.52	5.33	5.43	5.32
BCJ3	7.52	9.42	38.80	57.60	5.29	6.11	5.70	5.31
BCJ4	7.05	8.20	40.1	39.96	8.69	4.87	5.28	5.35
BCJ5	7.30	8.25	36.80	49.40	5.04	4.77	4.90	4.91
BCJ6	7.55	9.10	45.32	44.95	6.00	4.94	5.47	6.04
BCJ7	8.50	11.7	59.60	59.80	7.01	5.11	6.06	7.95

Note: Where, Δy = yield displacement, Δu = ultimate displacements, respectively, μ = displacement ductility factor, and μav.= average displacement ductility factor.

The displacement ductility of constructional RC sections guarantees sufficient deformation and early failure in either compression or tension zones (breaching of reinforcement or concrete crushing) or the required ductility of RC elements can be expressed in terms of the maximum displacement value (deformation max.) (Cohn & Riva, 1991). In most cases, it is suitable to express the deformations max from where of displacement ductility factors. The displacement ductility factor is defined as the deformation max divided by conformable deformation when reaching yielding during an earthquake (Park, 1989). The BCJ1 specimen is a ductile RC exterior joint that was designed based on the seismic provisions of ACI (ACI. 2014). The displacement ductility factor is μ= Δu/Δy where Δu: ultimate displacement, Δy: yield displacement, and drift ratio θu = Δu/L where L: length of the beam. Some accounts have been suggested to distinguish the yield point of the RC member, like equivalent energy account (Nie et al., 2020). As explained in Table 6, the displacements ductility of the BCJ2 - BCJ5 significantly increased by 6.26%,11.55%, 3.33%, 4.11%, 7.05%, and 18.59% compared with BCJ1 (control), respectively. Additionally, the ultimate drift ratio of specimens BCJ2-BCJ5 increased by 1.00%, 0.57%, 1.33%, 7.01%, 14.39%, and 50.56% compared with BCJ1, respectively. Generally, the ductility ratio improved after strengthening at the BFRP sheets.

Energy dissipation

Energy dissipated is calculated as one of the most important parameters to estimate seismic behavior at RC structures, and signals the capacity of RC structures to dissipate energy through inelastic displacements when exposed to seismic loads (Li et al., 2007), the cyclic loads in downward and upward directions, the energy dissipated was calculate through the zone surrounded into the load- displacement curves in all cycle Ei, as shown in Fig. 16. The cumulative dissipation of energy is realized by collecting regions via hysteretic curve reflation. The cumulative dissipation of energy by the control BCJ1 and BCJ2-BCJ7 specimens versus displacement is depicted in Fig. 17. Therefore, energy absorption increased with increasing displacement. The total cumulative dissipation of energy in specimens BCJ1, and BCJ2-BCJ7 was 4187.48, 4380.90, 5070.81, 4278.93, 4800.5, 5435.84 and 6452.62 kN.mm, which increased by 4.62%, 21.10%, 2.18 14.64 %, 29.81%, and 54.09% compared with BCJ1, respectively, as shown in Table 7.

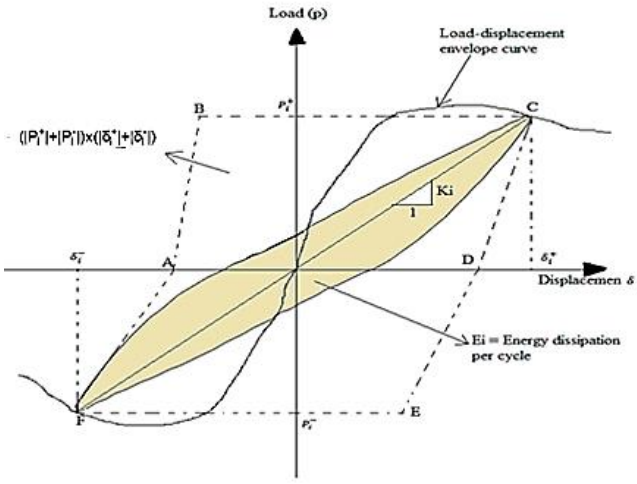

Fig. 16 Energy dissipation and stiffness

Stiffness degeneration

Stiffness joint K is the slope of the curve that the beam-column joins the ultimate load points in push and pull directions at all loops, and each drift ratio (ACI 34.1-05, 2005) It can be deduced from Eq. (1), as shown in Fig. 13.

$$K_i = \frac{|P_i^+|+|P_i^-|}{|\delta_i^+|+|\delta_i^-|} \quad (1)$$

where K_i is stiffness for every i cycle (KN/mm), Pi+ and Pi- are the maximum loads for every i cycle in the downward and upward direction, respectively, in KN; δi+ and δi- are the displacements of the maximum loads for every i cycle (mm). The comparison at the normalized stiffness of the BCJ1 specimen with BCJ2-BCJ7 strengthening specimens is shown in Fig. 18. The first stiffness at the BCJ1, and BCJ2-BCJ7 was 2.2, 2.34, 2.80, 2.4, 2.55, 2.87, and 2.95 KN/mm, which increased by 6.36%, 27.30%, 9.09%, 15.90, 30.45, and 34.10% compared with BCJ1 control, respectively, as shown in Table 7. The final stiffness for BCJ1-BCJ7 was, 0.35, 0.31, 0.44, 0.32, 0.36, 0.18, and 0.13 KN/mm, respectively, which increased by 11.43%, 25.71%, 8.57%, 2.85%, 48.55 and 62.86%, respectively, compared with the BCJ1 control. The first and final stiffness values increased with strengthening by FRP sheets, which was advantageous for RC buildings suffering from the surprised loss of stiffness under the influence of seismic (Borujerdi et al., 2021).

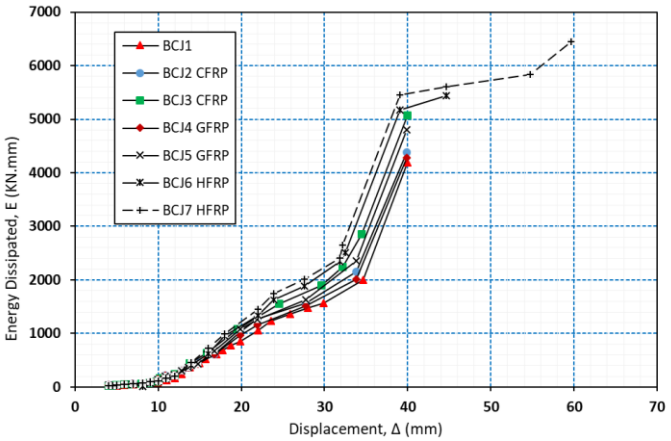

Fig. 17 Cumulative dissipated energy for BCJ1 and BCJ2-BCJ5 specimens

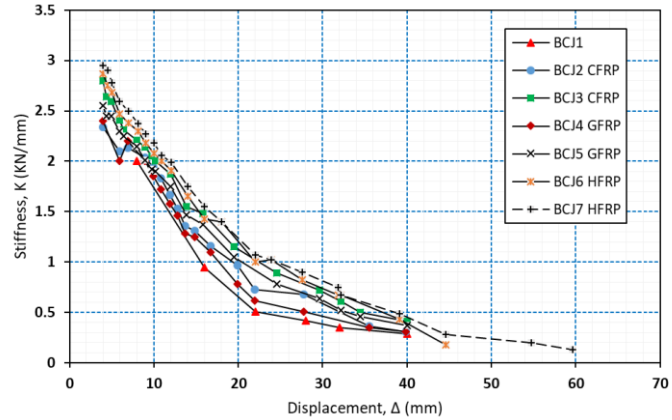

Fig. 18 Stiffness degeneration in all specimens

Table 7. Stiffness and energy results

Specimens	$K_{in.}$ (KN/mm)	($K_{in.}$ / BCJ1)	$K_{fi.}$ (KN/mm)	($K_{fi.}$ / BCJ1)	$E_{i.}$ (KN.mm)	($E_{i.}$ / BCJ1)
BCJ1	2.20	100%	0.35	100%	4187.5	100%
BCJ2	2.34	106.4%	0.31	88.6%	4380.9	104.6%
BCJ3	2.80	127.3%	0.44	125.7%	5070.8	121.1%
BCJ4	2.40	109.1%	0.32	91.4%	4278.9	102.2%
BCJ5	2.55	115.9%	0.36	102.9%	4800.5	114.6%
BCJ6	2.87	130.5%	0.18	51.5%	5435.8	129.8%
BCJ7	2.95	134.1%	0.13	37.1%	6452.6	154.%

Where, K_{in} = first secant stiffness, K_{fi}= final stiffness, E_i = cumulative energy

4.2 Numerical results and comparison to experimental results

To ensure the adequacy of the created numerical simulation in describing the behavior of RC exterior beam–column joints strengthened with fiber sheets, a detailed comparison between experimental and numerical results was established. Load-deflection diagrams; initial cracking loads; loads at failure; and crack patterns at failure were used as behavior indices. Since there were no strain gauges used in the experimental test, the maximum stress of the reinforcement and the fiber sheets can be inferred from the numerical results.

Model verification

Comparison between the load-displacement envelope plot obtained from finite element analysis with the experimental test results, also load verses deflection behavior was considered as a main parameter to verify the finite element model as shown in Fig. 19. Results comparison of the numerical analysis are compared with the experimental results for the joints in Table 8. The graph illustrates the similarities between numerical and experimental specimens. There is a discernible variation of nearly 9%–13%, which is explained by the size of the mesh and the intrinsic complexity of the non-linear modeling of hysteresis behavior.

Control joint (BCJ1)

The comparison shows the load-displacement envelope diagram of the analytical with experimental model BCJ1(control) in Fig. 19, the yield load obtained from finite element analysis at 7.1 KN is 12% more than the yield load of 6.25 KN obtained from the experimental study at this stage, the emergence of initial cracking. Similarly, the ultimate load obtained from finite element analysis at 21 KN is 11.70% more than the ultimate load of 18.87 KN from the experimental study at this stage, final failure event. At yield load, the displacement obtained in finite element analysis is 2.30 mm at beam end as compared to 2 mm which is 13% more than the experimental study. Similarly, at ultimate load, the displacement obtained infinite element analysis is 16.50 mm which is 11.5% more than the 14.80 mm of the experimental study. The deformation and the ultimate load are shown in Fig. 20 (a, b), Fig. 20 (c) shows the damage patterns and plastic hinge location also stress in the reinforcement bar reached 412 MPa.

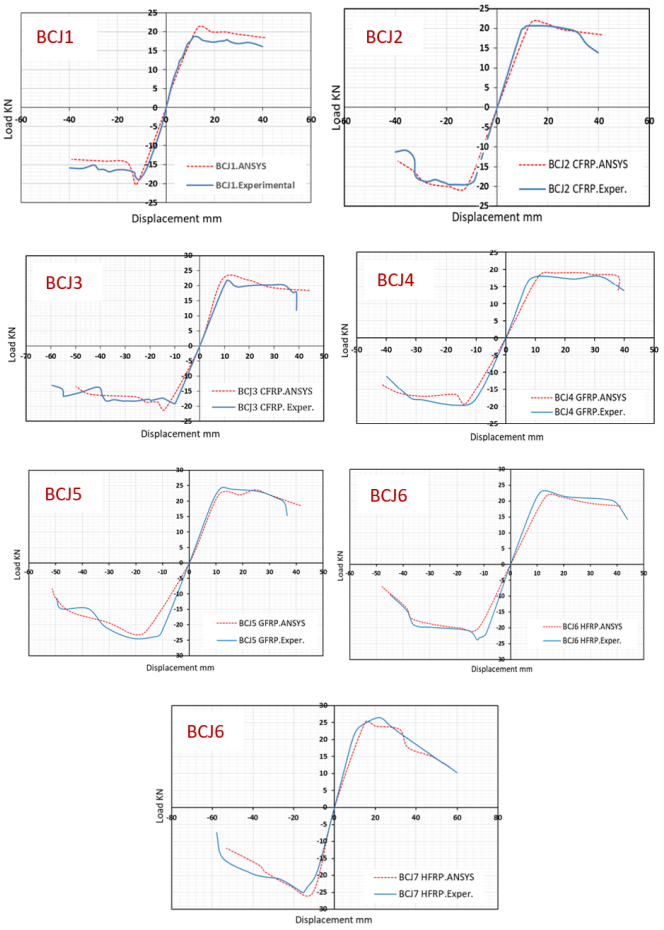

Fig. 19 Load-displacement envelope plot obtained from analytical with experimental study

Table 8. Comparison shows the results obtained from experimental study with numerical analysis for the joints

Specimen	Max. load (KN)		Percentage difference %	Displacement at Max. load (mm)		Percentage Difference %
	Experiment	Anys		Experiment	Anys	
BCJ1	18.87	21.0	11.28	39.91	44.1	10.49
BCJ2	20.63	23.2	12.34	39.99	41.2	9.65
BCJ3	21.50	24.0	11.63	40.00	44.1	10.25
BCJ4	18.10	19.1	12.43	37.33	38.1	10.79
BCJ5	24.38	23.7	11.19	49.00	51.3	9.97
BCJ6	23.35	21.2	9.29	44.00	48.0	9.09
BCJ7	26.87	25.0	10.68	59.88	56.0	9.68

Retrofitted specimen (BCJ2-BCJ7)

Fig. 19 illustrates the comparison of the load-displacement envelope diagram of the analytical with experimental model BCJ2. The yield load obtained from finite element analysis at 10.86 KN is 14.3% more than the yield load of 9.5 KN obtained from the experimental study at this stage, the emergence of initial cracking. Similarly, the ultimate load obtained from finite element analysis at 23.17 KN is 12.31% more than the ultimate load of 20.63 KN from the experimental study at this stage, final failure event, and small CFRP sheets tear. At yield load, the displacement obtained in finite element analysis is 3.91 mm at beam end as compared to 3.5 mm which is 11.71% more than the experimental study. Similarly, at ultimate load, the displacement obtained infinite element analysis is 13.52 mm which is 12.5% more than the 12 mm of the experimental study, the deformation and the crack at the ultimate load are shown in Fig. 21. The comparison shows the hysteretic load diagram of the analytical with experimental model BCJ3 in Fig. 19, the yield load obtained from finite element analysis at 14.73 KN is 13.31% more than the yield load of 13 KN obtained from the experimental study. Similarly, the ultimate load obtained from finite element analysis at 24 KN is 11.6% more than the ultimate load of 21.50 KN from the experimental study at this stage, final failure event, and large CFRP sheets tear. At yield load, the displacement obtained in finite element analysis is 5.68 mm at beam end as compared to 5 mm which is 13.6% more than the experimental study. Similarly, at ultimate load, the displacement obtained infinite element analysis is 13.25 mm which is 18.2% more than the 11.21 mm of the experimental study. The deformation and the crack at the ultimate load are shown in Fig. 21. The compared shows are the hysteretic load diagram of the analytical with experimental model BCJ4 in Fig. 19, the yield load obtained from finite element analysis at 10.54 KN is 9.22% more than the yield load of 9.65 KN obtained from the experimental study. Similarly, the ultimate load obtained from finite element analysis at 19.05 KN is 5% more than the ultimate load of 18.10 KN from the experimental study at this stage, final failure event, and small GFRP sheets tear. At yield load, the displacement obtained in finite element analysis is 4 mm at beam end as compared to 3.5 mm which is 14.3% more than the experimental study. Similarly, at ultimate load, the displacement obtained infinite element analysis is 11 mm which is 11.56% more than the 9.86 mm of the experimental study. The deformation and the crack at the ultimate load are shown in Fig. 21.

Figure 19 illustrates the comparison of the hysteretic load diagram of the analytical with experimental model BCJ5, the yield load obtained from finite element analysis at 11.13 KN is 8.58% more than the yield load of 10.25 KN obtained from the experimental study. Similarly, the ultimate load obtained from finite element analysis at 22.96 KN is 6% less than the ultimate load of 24.38 KN from the experimental study at this stage, final failure event, and large GFRP sheets tear. At yield load, the displacement obtained in finite element analysis is 3.83 mm at beam end as compared to 3.5 mm which is 9.42% more than the experimental study. Similarly, at ultimate load, the displacement obtained infinite element analysis is 14 mm which is 10.67% more than the 12.65 mm of the experimental study. The deformation and the crack at the ultimate load are shown in Fig. 21. The compared shows are the hysteretic load diagram of the analytical with experimental model BCJ6 in Fig. 19, the yield load obtained from finite element analysis at 11.10 KN is 9.41% less than the yield load of 11.8 KN obtained from the experimental study. Similarly, the ultimate load obtained from finite element analysis at 21 KN is 10% less than the ultimate load of 23.35 KN from the experimental study at this stage, final failure event, and small HFRP sheets tear. At yield load, the displacement obtained in finite element analysis is 4.53 mm at beam end as compared to 4 mm which is 13.25% more than the experimental study. Similarly, at ultimate load, the displacement obtained infinite element analysis is 13.76 mm which is 5.84% more than the 13 mm of the experimental study. The deformation and the crack at the ultimate load are shown in Fig. 21.

Comparison shows is the hysteretic load diagram of the analytical with experimental model BCJ7 in Fig. 19, the yield load obtained from finite element analysis at 15.69 KN is 10.34% less than the yield load of 17.5 KN obtained from the experimental study. Similarly, the ultimate load obtained from finite element analysis at 25 KN is 7% less than the ultimate load of 26.87 KN from the experimental study at this stage, final failure event, and large HFRP sheets tear. At yield load, the displacement obtained in finite element analysis is 6.11mm at beam end as compared to 7 mm which is 12.7% less than the experimental study. Similarly, at ultimate load, the displacement obtained infinite element analysis is 18.79 mm which is 9% more than the 20.85 mm of the experimental study. Fig. 21 shows the deformation and the crack at the ultimate load, as well as the stresses in the FRP sheets (stirrups shape). The final strength of FRP reached 3236 MPa, strain of FRP reached at 2.25%, strain of concrete reached at 1.75 %, and stresses in the reinforcement bar reached 618 MPa. The rapture of the FRP sheets was the final stage of the analysis.

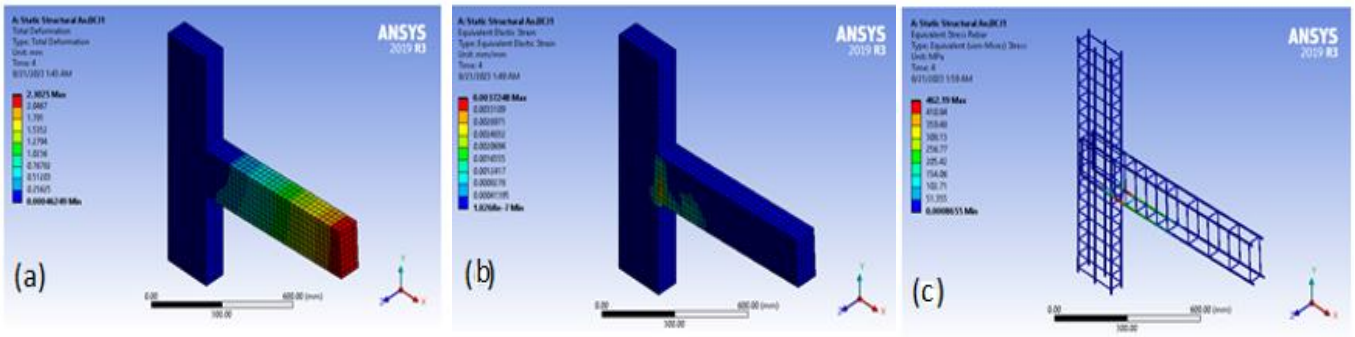

Fig. 20 The finite element outputs of BCJ1: a) Total deformation, b) FE crack pattern, c) bar stress

5. Conclusion

Seismic behavior of seven RC beam-column joints specimens was examined. Enhancement of confining using the FRP sheets was explored. Performance indices of six confined RC exterior joints under cyclic loading were compared to both control specimen's results and those from numerical models. The observations based on experimental and numerical study are summarized as follows:

The specimens strengthened with FRP show better performance than the unstrengthening specimens. The hybrid strengthening joints BCJ6 and BCJ7 exhibit higher stiffness and better response to cyclic loads.

The first cracking load was monitored to be increased at 47-64.29% for RC exterior joint specimens strengthened by HFRP sheets, 35.23-39% for those strengthened using GFRP sheets, and 34.21-52% for those strengthened by CFRP sheets compared with the BCJ1 control.

The maximum load with ultimate displacements of BCJ2-BCJ7 specimens increased to 8.53%, 12.23%, 4.25%, 22.60%, 19.18%, and 29.77% with 0.20%, 0.23%, 6.91%, 18.55%, 9.29%, and 33.35%, respectively, compared with the control specimen BCJ1. The maximum loads with displacement of the joints were increased by HFRP strengthening sheets.

Using large strips of 200 mm and 250 mm of FRP to safeguard the concrete by confinement and improve the ductility and capacity of the strengthened beam-column joints, in BCJ2-BCJ7 specimens, there was get better in displacement ductility ratios of 5.89%, 10.35%, 3.22%, 4.28%, 6.58%, and 15.67%, respectively, compared with the BCJ1 control.

The proposed strengthening techniques were considered to be touching during periods of energy dissipation because all BCJ2-BCJ7 strengthen specimens absorbed higher energy by 4.62%, 21.10%, 20.18%, 14.64%, 29.81%, and 54.10%, respectively, than reference specimen BCJ1. Using FRP strips to strengthen the joints was an effective method to improve the energy capacity, as in joints strengthened using large strips (CFRP, GFRP, or HFRP).

The first and final stiffness values show increases of 6.36 %, 27.30 %, 9.10 %, 15.90 %, 30.45 %, and 34.10 % or 11.43 %, 25.71 %, 8.57 %, 2.85 %, 48.55 %, and 62.86% for BCJ2-BCJ7 specimens, respectively, compared with the reference specimen BCJ1.

A comparison between results from numerical models and those resulting from experimental tests shows that the numerical analysis results are higher than the experimental results by 9.10-10.79% and 9.29-12.43%, for the ultimate displacement and ultimate load respectively.

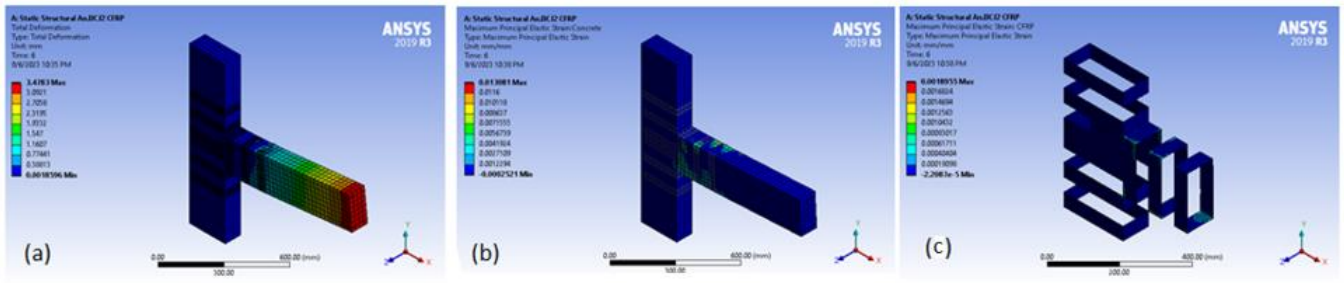

Specimen BCJ2

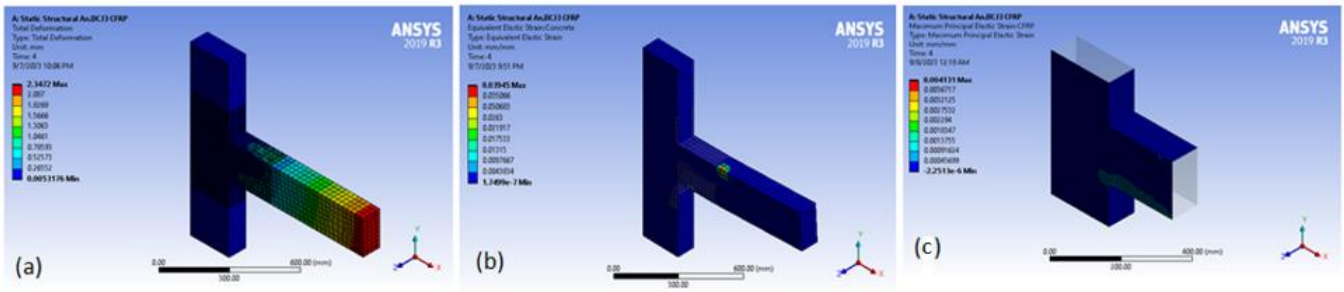

Specimen BCJ3

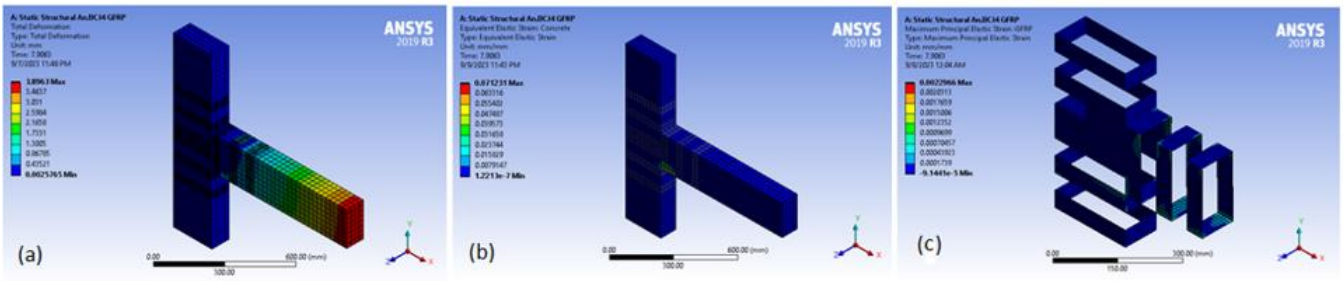

Specimen BCJ4

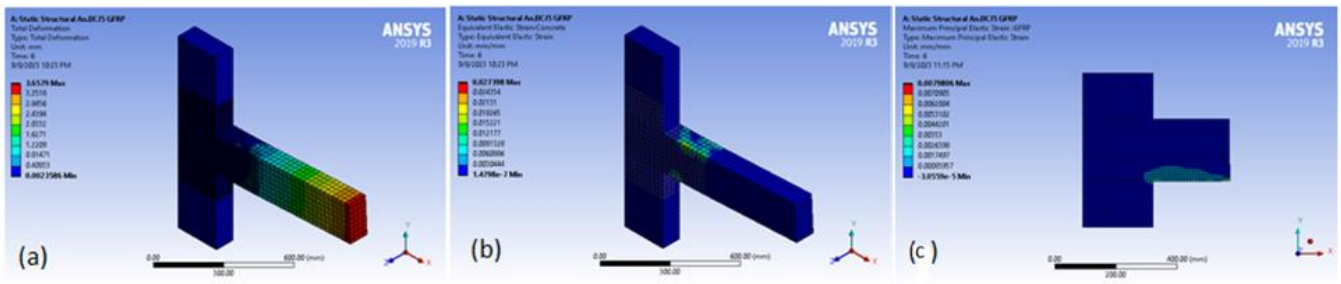

Specimen BCJ5

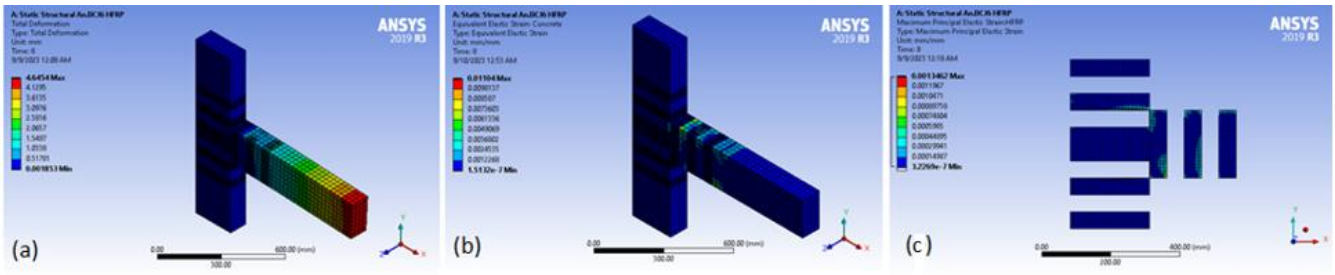

Specimen BCJ6

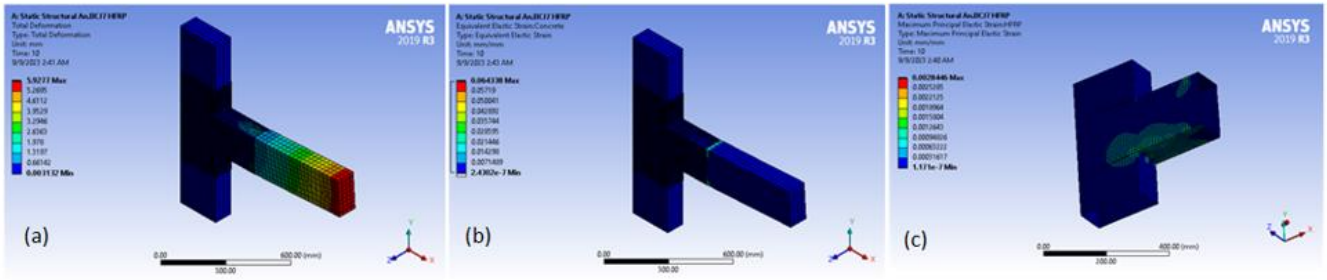

Specimen BCJ7

Fig. 21 The finite element outputs of BCJ2 – BCJ7: a) Total deformation, b-c) Equivalent elastic strain of the concrete and FRP

References

Aboelhassan, M. G. H. M. (2020). Behavior of precast reinforced concrete beam-column external connections under cyclic loading (Doctoral dissertation, Faculty of Engineering, Alexandria University). https://www.researchgate.net/profile/Mohamed-Aboelhassan-2/publication/353923189

Arowojolu, O., Ibrahim, A., Rahman, M. K., Al-Osta, M., & Al-Gadhib, A. H. (2019). Plastic hinge relocation in reinforced concrete beam–column joint using carbon fiber–reinforced polymer. Advances in Structural Engineering, 22(14), 2951-2965. https://doi.org/10.1177/1369433219855901

ACI, 374.1-05. Acceptance criteria for moment frames based on structural testing and commentary (ACI 374.1-05). ACI Committee 374: Farmington Hills, MI: American Concrete Institute (2005).

ACI. (2014). Building Code Requirements for Structural Concrete (ACI 318-14) and Commentary on Building Code Requirements for Structural Concrete (ACI 318R-14): American Concrete Institute (ACI), Detroit, Michigan, USA.

Akhlaghi, A., & Mostofinejad, D. (2020, December). Experimental and analytical assessment of different anchorage systems used for CFRP flexurally retrofitted exterior RC beam-column connections. In Structures (Vol. 28, pp. 881-893). Elsevier. https://doi.org/10.1016/j.istruc.2020.09.037

ACI-T1.1R-01. (2001). Acceptance Criteria for Moment Frames Based on Structural Testing (T1.1-01) and Commentary (T1.1R-01): ACI Innovation Task Group 1 and Collaborators.

Abdulkadir, M. R., Aziz, Z. A., & Muhammad, J. H. (2017). Nonlinear finite element analysis of reinforced concrete beams strengthened with externally bonded steel plate using ANSYS. Sulaimania Journal for Engineering Sciences, 4(4). https://www.iasj.net/iasj/article/163558

Borujerdi, A. S., Mostofinejad, D., & Hwang, H. J. (2021). Cyclic loading test for shear-deficient reinforced concrete exterior beam-column joints with high-strength bars. Engineering Structures, 237, 112140. https://doi.org/10.1016/j.engstruct.2021.112140

Barbhuiya, S., & Choudhury, A. M. (2015). A study on the size effect of RC beam–column connections under cyclic loading. Engineering Structures, 95, 1-7. https://doi.org/10.1016/j.engstruct.2015.03.052

Cohn, M. Z., & Riva, P. (1991). Flexural ductility of structural concrete sections. PCI journal, 36(2), 361-369. https://www.pci.org/PCI_Docs/Publications/PCI%20Journal/1991/March/Flexural%20Ductility%20of%20Structural%20Concrete%20Sections.pdf

De Risi, M. T., Del Vecchio, C., Ricci, P., Di Ludovico, M., Prota, A., & Verderame, G. M. (2020). Light FRP Strengthening of Poorly Detailed Reinforced Concrete Exterior Beam–Column Joints. Journal of Composites for Construction, 24(3), 04020014. https://doi.org/10.1061/(ASCE)CC.1943-5614.0001022

Esmaeeli, E. (2015). Development of hybrid composite plate (HCP) for strengthening and repair of RC structures (Doctoral dissertation, Universidade do Minho (Portugal)). https://search.proquest.com/openview/b9daf12f765d4f1439eae9e235be1c07/1

Elsouri, A. M., & Harajli, M. H. (2015). Repair and FRP strengthening of earthquake-damaged RC shallow beam-column joints. Advances in Structural Engineering, 18(2), 237-249. https://doi.org/10.1260/1369-4332.18.2.237

ECP203-2007. (2007). Egyptian Code for Design and Construction of Reinforced Concrete Structures (ECP203-2007): Housing and Construction National Research Center (HRPC), Cairo, Egypt.

ECP201-2012. (2012). Egyptian Code for Calculating Loads and Forces (ECP201-2012): Housing and Construction National Research Center (HRPC), Cairo, Egypt.

Faleschinia, F., Gonzalez-Librerosa, J., Zaninia, M. A., Zampieria, P &,.Pellegrinoa, C. (2017, September). Experimental Behavior of Damaged RC Beam-column Joints Repaired with FRP omposites. In presented on conference XVII Convegno ANIDIS-L'Ingegneria Sismica in Italia, At Pistoia (pp. 17-21). https://www.researchgate.net/profile/Flora-Faleschini/publication/319980753

Ghayeb, H. H., Razak, H. A., & Sulong, N. R. (2020). Performance of dowel beam-to-column connections for precast concrete systems under seismic loads: A review. Construction and Building Materials, 237, 117582. https://doi.org/10.1016/j.conbuildmat.2019.117582

Gnanapragasam, A. A., Chitra, G., & Ravi, S. R. (2016). Study on strengthening of rc beam column joint using hybrid FRP composites. Circuits and Systems, 7(10), 2846-2856. http://dx.doi.org/10.4236/cs.2016.710243

GAYAKE, S. B., & DHAKE, P. D. (2021). Structural behavior of beam column joint retrofitted using carbon fiber reinforced polymer. Journal of Materials and Engineering Structures «JMES», 8(1), 47-59.

Ilia, E., Mostofinejad, D., & Moghaddas, A. (2020). Cyclic behavior of strong beam–weak column joints strengthened with different configurations of CFRP sheets. Archives of Civil and Mechanical Engineering, 20(2), 1-26. https://doi.org/10.1007/s43452-020-0015-7

Javanmardi, M. R., & Maheri, M. R. (2017, November). Anisotropic damage plasticity model for concrete and its use in plastic hinge relocation in RC frames with FRP. In Structures (Vol. 12, pp. 212-226). Elsevier. https://doi.org/10.1016/j.istruc.2017.09.009

Kotsovou, G. M., Cotsovos, D. M., & Lagaros, N. D. (2017). Assessment of RC exterior beam-column Joints based on artificial neural networks and other methods. Engineering Structures, 144, 1-18. https://doi.org/10.1016/j.engstruct.2017.04.048

Khashi, K., Dehghani, H., & Jahanara, A. A. (2018). An optimization procedure for concrete beam-column joints strengthened with FRP. Iran University of Science & Technology, 8(4), 675-687.

Liu, W., & Jia, J. (2018). Experimental study on the seismic behavior of steel-reinforced ultra-high-strength concrete frame joints with cyclic loads. Advances in Structural Engineering, 21(2), 270-286. https://doi.org/10.1177/1369433217711

Laseima, S., Mutalib, A., Osman, S., & Hamid, N. (2021). Strengthening of deficient exterior rc beam-column joints using basalt fibre reinforced polymer sheets. Journal of Engineering Science and Technology, 16(5), 3687-3711.

Li, J., Gao, X., & Zhang, P. (2007). Experimental investigation on the bond of reinforcing bars in high performance concrete under cyclic loading. Materials and structures, 40, 1027-1044. https://doi.org/10.1617/s11527-006-9201-1

Mariselvam, T., & Sakthieswaran, N. (2015). Experimental Investigation on GFRP Wrapped RC Beam Column Joint. International Journal of Engineering Research (IJOER), 1.

Mosallam, A., Allam, K., & Salama, M. (2019). Analytical and numerical modeling of RC beam-column joints retrofitted with FRP laminates and hybrid composite connectors. Composite Structures, 214, 486-503. https://doi.org/10.1016/j.compstruct.2019.02.032

Marimuthu, S., & Sivasankara Pillai, G. (2021). Experimental investigation of exterior reinforced concrete beam-column joints strengthened with hybrid FRP laminates. Građevinar, 73(04.), 365-379. https://doi.org/10.14256/JCE.2765.2019

Mohanan, C., Abubaker, K. A., & Fathima, A. (2016). A Comparative Study of Retrofitting of Beam Column Joint Using Concrete jacketing, Steel Plate Jacketing, Glass Fiber wrapping.

Nawale, A., Mehetre, A. J., & Kandekar, S. B. (2015). Strengthening of RC Beam and Column Joint by Using CFRP &GFRP. International Journal of Scientific Engineering and Technology, 4(9), 457-460.

Nie, S., Zhou, T., Zhang, Y., Zhang, B., & Wang, S. (2020). Investigation on the design method of shear strength and lateral stiffness of the cold-formed steel shear wall. Mathematical Problems in Engineering, 2020, 1-13. https://doi.org/10.1155/2020/8959712

Okahashi, Y., & Pantelides, C. P. (2017). Strut-and-tie model for interior RC beam-column joints with substandard details retrofitted with CFRP jackets. Composite Structures, 165, 1-8. https://doi.org/10.1016/j.compstruct.2017.01.004

Ouyang, L. J., Gao, W. Y., Zhen, B., & Lu, Z. D. (2017). Seismic retrofit of square reinforced concrete columns using basalt and carbon fiber-reinforced polymer sheets: A comparative study. Composite Structures, 162, 294-307. https://doi.org/10.1016/j.compstruct.2016.12.016

Park, R. (1989). Evaluation of ductility of structures and structural assemblages from laboratory testing. Bulletin of the New Zealand society for earthquake engineering, 22(3), 155-166. https://www.bulletin.nzsee.org.nz/index.php/bnzsee/article/view/774

Rahim, K. A. N. A. (2019). Modelling of Reinforced Concrete Beam-column Joint for Cyclic Earthquake Loading. American Journal of Civil Engineering and Architecture, 7(2), 67-114. https://doi.org/10.12691/ajcea-7-2-4

Shayanfar, J., Bengar, H. A., & Parvin, A. (2018). Analytical prediction of seismic behavior of RC joints and columns under varying axial load. Engineering Structures, 174, 792-813. https://doi.org/10.1016/j.engstruct.2018.07.103

Sasmal, S., & Voggu, S. (2019). Nonseismic and seismic designed beam-column joints with rebar end anchors–Behaviour under reverse cyclic loading. Journal of Earthquake Engineering, 1-23. https://doi.org/10.1080/13632469.2019.1657990

Shen, D., Li, M., Kang, J., Liu, C., & Li, C. (2021). Experimental studies on the seismic behavior of reinforced concrete beam-column joints strengthened with basalt fiber-reinforced polymer sheets. Construction and Building Materials, 287, 122901. https://doi.org/10.1016/j.conbuildmat.2021.122901

Thompson, M. K., & Thompson, J. M. (2017). ANSYS mechanical APDL for finite element analysis. Butterworth-Heinemann.

Verderame, G. M., De Risi, M. T., & Ricci, P. (2018). Experimental investigation of exterior unreinforced beam-column joints with plain and deformed bars. Journal of Earthquake Engineering, 22(3), 404-434. https://doi.org/10.1080/13632469.2016.1233917

Wang, H., Marino, E. M., & Pan, P. (2019). Design, testing and finite element analysis of an improved precast prestressed beam-to-column joint. Engineering Structures, 199, 109661. https://doi.org/10.1016/j.engstruct.2019.109661

Zeng, L., Cui, Z., Xiao, Y., Jin, S., & Wu, Y. (2015). Cyclical behavior of concrete-encased composite frame joints with high strength concrete. Advances in Materials Science and Engineering, 2015. https://doi.org/10.1155/2015/873162

Zerkane, A. S., Saeed, Y. M., & Rad, F. N. (2019). Cyclic loading behavior of CFRP-wrapped non-ductile beam-column joints. Special Publication, 331, 34-54. https://doi.org/10.14359/51715592

Disclaimer